Pergamon

Bioorganic & Medicinal Chemistry 6 (1998) 151–161

BIOORGANIC & MEDICINAL CHEMISTRY

Probing the conformation of bilirubins with monopropionic analogs: a biological, spectroscopic, and molecular modeling study

Marcelo J. Kogan[a], María E. Mora[b], Josefina Awruch[b], José M. Delfino[a*†]

[a]*Departamento de Química Biológica, Facultad de Farmacia y Bioquímica, Universidad de Buenos Aires, Junín 956, 1113 Buenos Aires, Argentina*

[b]*Departamento de Química Orgánica, Facultad de Farmacia y Bioquímica, Universidad de Buenos Aires, Junín 956, 1113 Buenos Aires, Argentina*

Received 12 May 1997; accepted 28 August 1997

Abstract

The in vivo metabolism of a bilirubin analog substituted with a propionic acid chain in C_8 (**5**) showed that it is excreted in bile conjugated with glucuronic acid, while a positional isomer substituted with a propionate in C_7 (**6**) is excreted in bile without conjugation. A conformational analysis employing an optimized Monte Carlo method and a mixed Monte Carlo/stochastic dynamics reveals that isomer **5** adopts a 'ridge tile' conformation, stabilized by the presence of three intramolecular hydrogen bonds. On the contrary, isomer **6** exhibits a more closed structure, where impairment in the formation of at least one of the hydrogen bonds occurs. These theoretical predictions agree well with ^{1}H NMR, UV-vis, and TLC data.

Keywords: Bilirubins, glucuronidation, hydrogen bonds, molecular dynamics, Monte Carlo, conformational search.

1. Introduction

Bilirubin IXα is a pigment sparingly soluble in water. Its conjugation, mainly with glucuronic acid in the liver, is the third step in the metabolic sequence of heme IX degradation in mammals [1,2]. This biochemical modification confers greater polarity to the adduct, thus facilitating the excretion of the aglycon [3]. In fact, more than 97% of bilirubin IXα is present as the conjugate in the bile of human adults and rats.

Unconjugated bilirubin IXβ has also been detected in normal bile [4,5]. This compound is excreted mainly unconjugated, only 16% becomes an ester conjugate when normal Wistar rats were injected with bilirubin IXβ [6]. By contrast, since bilirubin IXβ is relatively more water soluble than the IXα isomer, it may not require conjugation in order to become excretable. Indeed, we have shown by perfusion of biliverdin IXβ through isolated rat liver that this pigment is exclusively excreted in its unconjugated form [7]. This opposite behavior between the positional isomers of bilirubin IX could in principle be attributed either to differential substrate recognition by the UDP-sugar transferases and/or to the physicochemical properties (e.g. polarity) of each isomer.

There is support for the notion that the physicochemical characteristics (e.g. solubility) of bilirubins depend on the conformation of these molecules, which, in turn, are mainly determined by the tendency to form intramolecular hydrogen bonds [8]. In this regard, folded 'ridge tile' structures were proposed as minimum energy conformers for analogs of bilirubin IXα on the basis of experimental (X-ray diffraction; UV-vis, NMR, and CD spectroscopies) and theoretical evidences

*Corresponding author.
†Tel: (541) 962 5506 or (541) 964 8291; fax: (541) 962 5457; e-mail: rtdelfin@criba.edu.ar

0968-0896/98/$19.00
PII: S0968-0896(97)10015-3

(conformational analyses by energy minimization and molecular dynamics). This folded conformation, stabilized by the formation of intramolecular hydrogen bonds between the propionic carboxyl and the lactamic and pyrrolic NHs, seems to be important for bilirubin glucuronidation [8,9].

On the other hand, it was demonstrated that the presence of two carboxyl groups in the molecule is not an essential feature for bilirubin binding to the active site of UDP-sugar transferases [10]. We introduce here analogs of bilirubin endowed with single propionic acid chains and, therefore, appropriate for probing structural features relevant for glucuronidation. Further insight into the preferred conformations of these analogs and the importance of intramolecular hydrogen bonding was obtained by molecular mechanics simulations. Results from our theoretical calculations are discussed in the context of experimental data from in vivo excretion of these pigments, from their polarity, as measured by TLC, and from ^{1}H NMR and UV-vis spectroscopies.

2. Results and discussion

2.1 Design, synthesis and physicochemical properties of analogs of bilirubin

We chose to study analogs of bilirubin substituted on C_7 or C_8 with a single propionic chain. We synthesized and characterized compounds **5** and **6** (Scheme 1), and measured their ability to form glucuronides in vivo. According to a current hypothesis [8], substitution at C_8 would lead to the formation of three hydrogen bonds, whereas the propionic acid chain attached to C_7 would impair intramolecular hydrogen bonding.

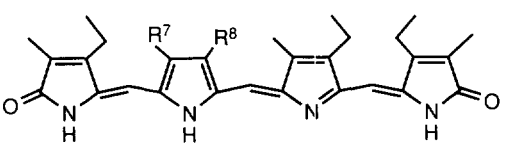

1-4

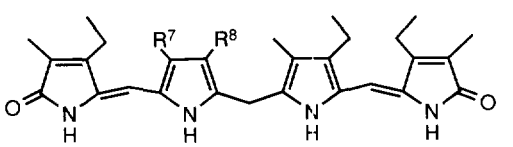

5-6

1 $R^7 = CH_3$; $R^8 = CH_2CH_2CO_2CH_2CH_3$
2 $R^7 = CH_2CH_2CO_2CH_2CH_3$; $R^8 = CH_3$
3, 5 $R^7 = CH_3$; $R^8 = CH_2CH_2CO_2H$
4, 6 $R^7 = CH_2CH_2CO_2H$; $R^8 = CH_3$

Scheme 1.

Bilirubins **5** and **6** were prepared by reduction of the corresponding biliverdins **3** and **4**. In turn, these compounds were obtained by saponification of biliverdin methyl (or ethyl) esters **1** and **2** (Scheme 1), which were prepared by total synthesis as described elsewhere [11].

Compound **5** (R_f 0.86) is less polar than compound **6** (R_f 0.77), and both are less polar than the natural bilirubin IXα (R_f 1).

Basically, we focused the analysis of the ^{1}H NMR spectra (taken in chloroform) of compounds **5** and **6** on the chemical shifts of signals corresponding to the NHs and the carboxyl OH, since the presence or absence of hydrogen bonds can be monitored by the position of these resonances. Compound **5** exhibits the following signals: 13.6 ppm for the acidic OH, 10.35 and 8.0 ppm for the lactamic NHs, and 8.7 and 7.74 ppm for the pyrrolic NHs. For compound **6**, the corresponding data are the following: 13.20, 10.25 and 9.57; 9.98 and 8.00 ppm. Our assignment of resonances agrees well with values reported by others [12] for similar compounds, where the identity of each proton was ascertained by H/D exchange experiments.

The UV-visible spectrum in chloroform of compound **5** shows a band with an absorption maximum at 410 nm, which closely resembles that of mesobilirubin XIIIα. By contrast, the spectrum of isomer **6** is blue-shifted, with a maximum at 392 nm, close to the value observed for mesobilirubin IVα [13].

2.2 Biological assays in vivo

Compounds **5** and **6** were injected in the bloodstream of male Wistar rats in order to test their excretion in bile. The analysis by TLC of bilirubin components present in this fluid showed that **5** and **6** were indeed excreted at a level which reaches 15 and 27%, respectively, of the values observed for total endogenous bilirubin IXα (Table 1). However, a qualitative difference is readily apparent: compound **6** is almost exclusively excreted as the unconjugated form (R_f 0.77), whereas bilirubin **5** appears in bile entirely as the monoglucuronide (R_f 0.58).

On the other hand, both bilirubin analogs are rapidly cleared from rat bile, mostly before 30 min. No detectable levels of any of these compounds are seen after 60 min. At all time points tested, no observable difference was seen in the relative proportion of conjugated versus unconjugated forms for endogenous bilirubin, regardless of whether any of the exogenous compounds were or were not injected. This result means that the clearance system of bilirubins is not affected by the load of the analogs.

The monoglucuronide of compound **5** is a novel biosynthetic product, which was characterized by its TLC behavior and by FAB mass spectrometry. Bilirubin IXα monoglucuronide (R_f 0.46) is more polar than the

Table 1
In vivo excretion of analogs of bilirubin in rat bile

Time (min)	Concentration of bilirubin analog (nmol of bilirubin per ml of bile ± S.E.)[a]			
	5	glucuronide of **5**	**6**	glucuronide of **6**
0	—[b]	—	—	—
30	—	4.01 ± 1.10	8.32 ± 1.65	—
60	—	2.28 ± 0.94	1.59 ± 0.57	—
90	—	—	—	—

[a]Data for each analog assayed are expressed as the mean value ± standard error of four independent experiments. Bile (0.35 ± 0.05 ml) was collected at each time point. Samples at time 0 min represent bile collected for 30 min previous to the injection of each analog.
[b]Non detectable levels of bilirubin are denoted with the symbol '—'. The concentration (nmol/ml) of endogenous free bilirubin IXα, its monoglucuronide and its diglucuronide for control rats (no analog injected) and experimental animals (compound **5** or **6** injected) were the following: 0.99 ± 0.45, 24.66 ± 2.10. 11.39 ± 1.90 for control rats; 0.94 ± 0.07, 18.51 ± 1.67, 7.48 ± 0.50 for rats injected with **5**; and 1.06 ± 0.10, 20.29 ± 0.84, 9.82 ± 0.60, for rats injected with **6**. For details see the Experimental section.

monoglucuronide of compound **5** (see above), as expected by the absence of one propionic acid chain in the latter. The FABMS of this compound (using thioglycerol as matrix) exhibits a signal corresponding to the base peak at *m/z* 543, whereas the molecular ion peak is small (*m/z* 719, M^+-H, 17%), due to cleavage of the glycosidic bond. By comparison, bilirubin analog **6** (using 3-nitro-benzyl alcohol as matrix) showed the molecular ion peak at *m/z* 544 (M^+, 100%).

2.3 Conformational analysis

2.3.1 Optimized Monte Carlo search, energy minimization and relative stability of isomers

Molecular models for compounds **5** and **6** were initially constructed using the model-building facility implemented in MacroModel [14]. Coordinates for these structures were used as input for BatchMin, the calculation module of this program.

In order to search the conformational space available to these compounds, we ran an optimized Monte Carlo protocol that allowed free rotation around all dihedral angles (Φ_1 through Φ_8, Fig. 1) which constitute the major determinants of the structure. A conformational search of bilirubin analogs **5** and **6** was carried out with BatchMin, starting from four planar structures, where the Φ_1,Φ_2 central pair of torsions adopted the following values: 0,180; 180,0; 0,0 and 180,180°. All the other dihedral angles were as shown in Fig. 1. Structures corresponding to the energy minima (as calculated with the force field MM2*) within a 6 kcal/mol window above the global minimum are shown in Table 2. In order to calculate the heats of formation of **5** and **6**, these structures were used as input for the semiempirical method AM1, as implemented in HyperChem [15]. After convergence is reached, a single point calculation was run to yield these values (Table 2).

In order to validate this approach on bilirubins, we ran a test calculation (100,000 steps) on bilirubin IXα, allowing free rotation around the central pair Φ_1, Φ_2 and around all torsions along the two propionic acid chains. The starting geometry was 'porphyrin-like' (i.e. $\Phi_1,\Phi_2 = 0,0°$) and an all transoid conformation for the propionic acid chains. As a result, we obtained a global minimum structure which did not differ significantly from that found by others [8] or the crystallographic structure [16,17].

Regardless of the choice of the initial structure, the conformational search of isomer **5** yielded three distinct nonenantiomeric conformers (Table 2). The global minimum structure of this analog ($\mathbf{5_1}$) adopts a typical 'ridge tile' conformation (Fig. 2). Conformer $\mathbf{5_2}$ is very close in shape to $\mathbf{5_1}$, except mainly for a difference at the central Φ_2 torsion.

Structures $\mathbf{5_1}$ and $\mathbf{5_2}$ show the presence of three hydrogen bonds (Table 2). The nonbonded distances $CO_8^3...H_{23}N$, $CO_8^3...H_{24}N$ and $OH_8^5...O_{19}C$ fall within acceptable limits for hydrogen bonding.

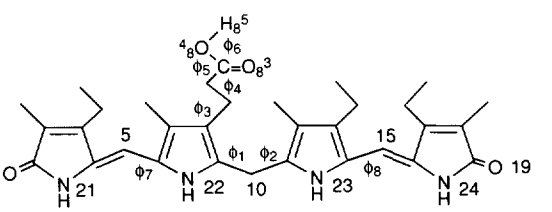

5

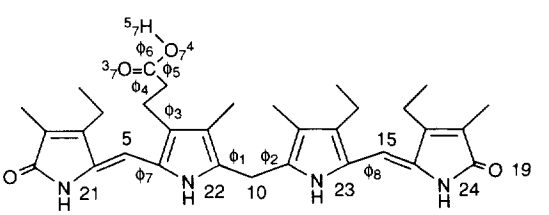

6

Fig. 1. Structure of bilirubin analogs **5** and **6** showing the torsion angles determining the conformation.

Likewise, it can be seen that the dihedral angles determining the conformation of the propionic acid chain in these conformers (i.e. Φ_3 and Φ_4) diverge from the ideally expected values (i.e. ±90 and 180°, respectively). In fact, both angles orient the end of the propionic side chain towards the opposite dipyrrinone, favoring the formation of the intramolecular hydrogen bonds, despite the increased steric hindrance.

The higher energy conformer $\mathbf{5_3}$ (6.7 kcal/mol over the global minimum) is more extended and flatter than $\mathbf{5_1}$ or $\mathbf{5_2}$. In spite of this fact, this structure is still capable of forming three intramolecular hydrogen bonds, albeit

Table 2
Conformations corresponding to energy minima for compounds **5** and **6**[a]

Conformer[a] Dihedral angle (°)[c]	$\mathbf{5_1}$	$\mathbf{5_2}$	$\mathbf{5_3}$[b]	$\mathbf{6_1}$	$\mathbf{6_2}$	$\mathbf{6_3}$
Φ_1	55.7 (52.0)	58.0 (58.5)	−118.0 (−114)	−42.0 (−51.2)	79.9 (84.0)	−90.0 (−82.5)
Φ_2	75.2 (78.6)	47.4 (50.6)	−112.5 (−112)	−41.9 (−29.5)	68.2 (67.0)	40.6 (34.8)
Φ_3	120.5 (121.5)	120.0 (112.8)	79.4 (81.2)	96.8 (112.8)	−82.3 (−77.7)	99.2 (114.2)
Φ_4	−53.2 (−62.5)	−59.0 (−74.9)	−141 (−138)	−50.4 (−57.0)	−59.7 (−64.2)	−43.0 (−57.6)
Φ_5	−12.6 (−28.4)	4.1 (−8.6)	67.2 (77.4)	82.0 (99.0)	75.7 (105.7)	96.0 (109.4)
Φ_6	−179.3 (−177.9)	179.0 (179.7)	169.0 (175.0)	−179.0 (178.1)	−176.0 (−177.0)	179.0 (177.3)
Φ_7	−36.6 (30.2)	35.1 (33.8)	36.7 (31.8)	32.1 (32.9)	33.4 (29.3)	43.4 (37.8)
Φ_8	−28.4 (−26.8)	26.2 (24.8)	33.4 (33.3)	21.5 (13.2)	−31.2 (−27.9)	−33.4 (−33.4)
Distance (Å)[c]						
CO...H_{23}N	1.906 (2.161)	1.870 (2.231)	1.939 (2.182)	2.816 (2.979)	3.633 (3.887)	3.145 (4.002)
CO...H_{24}N	1.890 (2.192)	1.882 (2.181)	1.917 (2.174)	1.994 (2.152)	1.898 (2.191)	1.971 (2.192)
OH...O_{19}C	1.715 (2.113)	1.720 (2.122)	1.740 (2.148)	1.696 (2.082)	1.702 (2.086)	1.689 (2.127)
Energy (H_f[d]) (kcal/mol)	12.08 (−82.70)	13.22 (−83.53)	18.70 (−79.33)	13.30 (−79.57)	15.75 (−80.19)	16.94 (−79.17)

[a]All minima within a 6 kcal/mol window above the global minimum are recorded. After visual inspection of each structure, only non-superimposable and non-enantiomeric conformers are described.

[b]Conformer $\mathbf{5_3}$ appears when the energy barrier above the global minimum is increased to 7 kcal/mol.

[c]The definition of dihedral angles follows the convention: Φ_1: $N_{22}C_9C_{10}C_{11}$; Φ_2: $N_{23}C_{11}C_{10}C_9$; Φ_3: $C_9C_8C_8{}^1C_8{}^2$ (**5**) or $C_6C_7C_7{}^1C_7{}^2$ (**6**); Φ_4: $C_8C_8{}^1C_8{}^2C_8{}^3$ (**5**) or $C_7C_7{}^1C_7{}^2C_7{}^3$ (**6**); Φ_5: $C_8{}^1C_8{}^2C_8{}^3O_8{}^3$ (**5**) or $C_7{}^1C_7{}^2C_7{}^3O_7{}^3$ (**6**); Φ_6: $C_8{}^2C_8{}^3O_8{}^4H_8{}^5$ (**5**) or $C_7{}^2C_7{}^3O_7{}^4H_7{}^5$ (**6**); Φ_7: $N_{22}C_6C_5C_4$; Φ_8: $N_{23}C_{14}C_{15}C_{16}$. Hydrogen bond distances correspond to the following: CO...H_{23}N: $CO_8{}^3$...H_{23}N (**5**) or $CO_7{}^3$...H_{23}N (**6**); CO...H_{24}N: $CO_8{}^3$...H_{24}N (**5**) or $CO_7{}^3$...H_{24}N (**6**); OH...O_{19}C: $OH_8{}^5$...O_{19}C (**5**) or $OH_7{}^5$...O_{19}C (**6**). Values represent dihedral angles and bond distances obtained after the MC optimized method [32] employing the MM2* force field. The corresponding values after energy minimization by the semi-empirical method AM1 are reported between parentheses.

[d]Energy values calculated after molecular mechanics (MM2*) are reported as differences with respect to the global minimum. Heats of formation (H_f) calculated with AM1 are shown between parentheses.

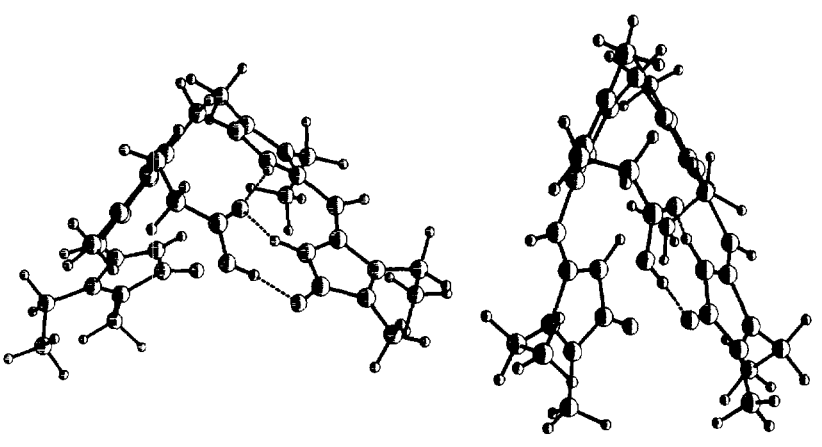

Fig. 2. Ball and stick conformational representation of minimum energy conformers of compounds **5** and **6** obtained after the optimized MC search. Dotted lines represent hydrogen bonds.

at the expense of an increment in torsional energy and a decrease in the electrostatic attraction (data not shown). Correspondingly, the heat of formation of this conformer, calculated by AM1, is more than 3 kcal/mol higher than for conformer $\mathbf{5_1}$.

On the other hand, the conformational search of isomer **6** gave three nonenantiomeric conformers, whose torsion angles are shown in Table 2. The global minimum conformer $\mathbf{6_1}$ shows a somewhat more closed structure, as depicted in Fig. 2. The interatomic distance between the lactamic oxygens is 8.2 Å in conformer $\mathbf{5_1}$ and 4.6 Å in $\mathbf{6_1}$. All conformers of **6** exhibit folded structures, with less tendency to form intramolecular hydrogen bonds. In fact, none of these conformers allow the formation of the $CO_7^3...H_{23}N$ hydrogen bond. In correspondence with this observation, $\mathbf{6_1}$ is ca. 3 kcal/mol less stable than $\mathbf{5_1}$, as evidenced by the difference in their heats of formation.

The conformers corresponding to the global minima of both bilirubin analogs ($\mathbf{5_1}$ and $\mathbf{6_1}$) were compared with bilirubin IXα (Table 3). As expected, $\mathbf{5_1}$ shows a conformation which more closely resembles bilirubin IXα than the positional isomer $\mathbf{6_1}$.

A similar set of conformers for each bilirubin analog were obtained when we restricted the rotational degrees of freedom to angles Φ_1 through Φ_6, implying that peripheral torsions Φ_7 and Φ_8 do not impose restrictions on the overall shape of the energy minimum conformations.

In many cases, a simulated annealing protocol [18] run for 50 ps on each local energy minima, where the initial and final temperatures were set at 300 and 50 K, respectively, yielded the global minimum as the sole output structure. An independent conformational search employing the AMBER* force field instead of MM2* produced the same set of conformers for both isomers. Rigid body superimpositions of the corresponding global energy minima calculated with each force field resulted in RMS values of 0.226 Å for compound **5** and 0.333 Å for compound **6**. After the AM1 method was applied to these structures, we noticed the following points: (i) the central pyrrol rings are closer to perfect planarity, as compared to the outer rings, in agreement with observations made by others [19] for bilirubin IXα; (ii) the calculated distances for the intramolecular hydrogen bonds are uniformly greater than those estimated by MM2*; (iii) C_5C_6 and $C_{14}C_{15}$ bonds exhibit essentially single bond character, whereas bond distances C_4C_5 and $C_{15}C_{16}$ are consistent with pure double bond character (results not shown).

Table 3
Comparison of energy minima conformers of compounds **5**, **6**, and bilirubin IXα

Compound		RMS deviation after a rigid body superimposition (Å) Bilirubin IXα[a]		
5	Conformer	$\mathbf{5_1}$	$\mathbf{5_2}$	$\mathbf{5_3}$
		0.427	0.937	1.898
6	Conformer	$\mathbf{6_1}$	$\mathbf{6_2}$	$\mathbf{6_3}$
		1.667	1.281	1.240

[a]Only the coordinates of the tetrapyrrole skeleton (i.e. the tetrapyrrole system without substituents) are compared.

Our calculated hydrogen bond distances and angles agree well with those reported by others [19] for bilirubin IXα employing AM1 and PM3. It is noteworthy that these semiempirical methods consistently predict larger bond distances and smaller bond angles than those observed experimentally by crystallography.

2.3.2 Mixed Monte Carlo/stochastic dynamics

The aim of this study was to evaluate the extent of intramolecular hydrogen bonding in the conformational ensemble corresponding to each bilirubin analog. We believe that this characteristic is a key factor determining both structure and properties of each compound. Towards this end, we applied a recently developed MC/SD method [20].

In order to run each simulation (3 ns) using a reasonable computer time and still be able to meet the convergence criteria discussed below, the application of this method on our bilirubin analogs required a reduction in the number of allowed torsions. Thus, free rotation was allowed only around Φ_1 through Φ_6 (Fig. 1), since these angles are the key determinants of the final overall conformation (see above). Several runs following the

Table 4
Most frequent dihedral angles for compounds **5** and **6** encountered along the MC/SD simulation [a]

Conformer Dihedral angle (°)[b]	Compound **5**	Compound **6**
Φ_1	60 (50, 70)	−80 (−55, −100)
Φ_2	75 (50, 90)	−5 (−40, 40)
Φ_3	115 (105, 130)	95 (70, 115)
Φ_4	−55 (−40, −70)	−45 (−35, −60)
Φ_5	0 (−20, 20)	75 (50, 100)
Φ_6	180 (−160, 165)	100 (70, 130)

[a]MC/SD simulations at 300 K in chloroform employing the AMBER* force field were run for 3 ns. This time allows the calculation to converge according to the criteria mentioned in the Experimental section. Two hundred thousand conformers were sampled for each isomer.

[b]The definition of dihedral angles follows the conversion described in the legend to Table 2. The values represent bond angles for the most populated states (mode), the limits for the width of the distribution bell at half height are reported between parentheses. For all angles, no other value was observed to be significantly populated.

protocol described below were carried out starting from: (i) the two enantiomers of the global energy minimum conformers $\mathbf{5_1}$ and $\mathbf{6_1}$, (ii) 'extended' structures ($\Phi_1,\Phi_2 = 180,180°$), or (iii) 'porphyrin-like' structures ($\Phi_1,\Phi_2 = 0,0°$). In all cases, average values for hydrogen bond distances and angles calculated on the final conformational ensemble were the same (results not shown).

After an initial equilibration period of 50 ps, each simulation was allowed to proceed for 3,000 ps at 300 K and produced as output a population of 200,000 conformers. This protocol ensures that the following convergence criteria are met: (i) the final average values for bond distances and bond angles are the same, regardless of the choice of starting structure; (ii) mean temperature and mean enthalpy reach numerical stability; and (iii) a symmetrical distribution for all freely rotating dihedral angles is observed.

Table 5
Relative tendency to form hydrogen bonds for compounds **5** and **6**

Hydrogen bond	Compound **5**	Compound **6**
CO...H_{23}N		
Distance (Å)[a]	1.85 (0.20)	2.80 (0.40)
N–H...O angle (°)[a]	152 (17.5)	162 (25)
H...O=C angle (°)[a]	162 (15)	147 (27.5)
%av. (%−, %+)[b]	91 (77, 94)	12 (3, 12)
CO...H_{24}N		
Distance (Å)[a]	1.85 (0.15)	2.05 (0.30)
N–H...O angle (°)[a]	147.5 (15)	132.5 (15)
H...O=C angle (°)[a]	132.5 (15)	142.4 (17.5)
%av. (%−, %+)[b]	93 (81, 95)	60 (33, 70)
OH...O_{19}C		
Distance (Å)[a]	1.85 (0.15)	1.75 (0.20)
O–H...O angle (°)[a]	167.5 (12.5)	162.5 (15)
H...O=C angle (°)[a]	122.5 (10)	132.5 (15)
%av. (%−,%+)[b]	91 (84, 92)	94 (90, 94)

MC/SD simulations at 300 K in chloroform employing the AMBER* force field were run for 3 ns. This time allows the calculation to converge according to the criteria mentioned in the Experimental section. Two hundred thousand conformers were sampled for each isomer.

[a]The convention for bond distances and angles was stated in the legend to Table 2. These values correspond to the most populated states (mode), the half-width of the distribution bell at half height is reported between parentheses.

[b]Population of H-bonded conformations, as estimated on each conformer found along the run. By definition, the H-bond X–H...Y–Z should meet the following criteria: average values (%av) were calculated for a H...Y distance < 2.5 Å, X–H...Y angle > 120° and H...Y–Z angle > 90°; %+ values result from a less stringent definition of the H-bond, namely, an H...Y distance < 2.75 Å, X–H...Y angle > 108° and H...Y–Z angle > 81°; %−values result from a more stringent definition, namely, an H...Y distance < 2.25 Å, X–H...Y angle > 132° and H...Y–Z angle > 99°.

The most frequent values of $\Phi_1 - \Phi_6$ found along the MC/SD run are reported in Table 4. For compound **5**, a close agreement is observed between these values and those characteristic of the global minimum $\mathbf{5_1}$ (Table 2). For compound **6**, the correspondence is less strict. Taken together, these facts reveal that the conformational ensemble for **5** is well represented by the structure of the global minimum $\mathbf{5_1}$. By contrast, for compound **6**, larger excursions are permitted, as evidenced by the larger width of the distributions, in particular for the critical torsions Φ_1 and Φ_2.

The evidence presented in Table 5 indicates that while compound **5** is able to form all three intramolecular hydrogen bonds in chloroform at 300 K, an impairment in the formation of the $CO_7{}^3...H_{23}N$ and $CO_7{}^3...H_{24}N$ bonds is found for compound **6**. The biggest effect is seen for the former bond. Depending on the stringency of the criterion used for the definition of the hydrogen bond, the actual calculated percentages vary within narrow limits. As expected, average bond distances obtained after MC/SD are slightly larger than those observed in the global minima. Qualitatively, these results are consistent with the extra strain observed for the energy minimized structures corresponding to isomer **6** (see Table 2).

2.4 The position of the propionic acid chain in bilirubins determines both its biological and physicochemical properties

The structure of bilirubins determines their ionization, solubility, bonding to serum proteins and bile salts, their interaction with biological membranes, and their conjugation and biliary excretion [21]. In particular, bilirubins adopt conformations which favor their glucuronidation, thus making them excretable through the liver into the bile [8]. Modification of the carboxylic group position across the tetrapyrrole system influences molecular lipophilicity, a property which is generally attributed to the presence of intramolecular hydrogen bonding [6,7]. (See also references cited in Ref. 6).

In agreement with these notions, we observed a clear-cut difference in the conjugation behavior of two monopropionic bilirubin analogs which differ in the position of the substituent (Fig. 1 and Table 1). It appears that compound **5** requires glucuronidation in order to be excreted. Conversely, compound **6** appears in bile without modification. These facts are consistent with the more lipophilic character observed for **5**, as evidenced by its TLC behavior. These data suggest that the physicochemical properties of bilirubins might play a critical role in the recognition by the UDP-sugar transferase. However, the overall conformation of the molecules as well as the position of the carboxyl group in bilirubins could also be important factors. Definite evidence in this regard should await results from in vitro studies, which are currently in progress.

In bilirubins, the ^{1}H NMR chemical shifts of pyrrolic and lactamic NHs provide a useful way to determine whether the dipyrrinone moieties participate in intramolecular hydrogen bonding. The pattern of these signals observed for compound **5** dissolved in chloroform, i.e. the lactamic and pyrrolic NHs at δ 10.35 and 8.7 ppm, respectively, agrees well with that found for a similarly substituted analog described recently [12] and closely resembles that observed for mesobilirubin XIIIα and bilirubin IXα [22–24]. Likewise, the pattern of signals of isomer **6** occurs at similar chemical shifts to those found for a previously reported monopropionic analog at C_7 [12]. Taken together, these evidences indicate that **5** is capable of forming both hydrogen bonds involving the NHs, whereas in **6**, at least the hydrogen bond involving the pyrrolic NH cannot be present. In addition, both **5** and **6** show signals at δ 13.6 and 13.2 ppm, respectively, which were assigned to the OH participating in the CO...HO hydrogen bond. We believe that the different environment around this bond in isomer **6** may explain the lower chemical shift. By comparison, a value of 12 ppm was observed for compounds where this OH does not participate in intramolecular H-bond [24].

In order to explain these data, a conformational difference between **5** and **6** should account for the different tendency to establish an intramolecular hydrogen bond network. Results from molecular modeling presented in this paper support this notion.

Moreover, the UV-visible spectrum of **5** (λ_{max} at 410 nm) closely resembles that of mesobilirubin XIIIα (substituted at C_8), suggesting a similarity in the conformation of these compounds. By contrast, isomer **6** exhibits a maximum at 392 nm, similarly to mesobilirubin IVα (substituted at C_7). It may be argued that the red shift observed in **5** could be taken as an indicator of a less folded conformation [24]. Conversely, the more folded conformation of **6** determines that the dipyrrinone chromophores be oriented with nearly parallel transition dipoles.

2.5 Molecular modeling reveals a key role for intramolecular hydrogen bonds in stabilizing the conformation of bilirubins

After a Monte Carlo conformational search and energy minimization, the most likely structures (global minima) for compounds **5** and **6** were found. While both isomers adopt folded structures, differences are evident as regards overall shape and intramolecular hydrogen bonding, which bring about a difference in stability.

Isomer **5** adopts a 'ridge tile' conformation stabilized by the presence of three intramolecular hydrogen bonds, namely, a bifurcated bond between the propionic carbonyl and the pyrrolic and lactamic NHs and a single bond between the propionic hydroxyl and the lactamic carbonyl. On the contrary, isomer **6** presents a somewhat more closed structure (i.e. where the interplanar angle between the two dipyrrinone moieties is smaller, Fig. 2). Here an impairment in the formation of at least one of the three hydrogen bonds occurs (i.e. the distance between the propionic carbonyl and the pyrrolic NH is inconsistent with the formation of a hydrogen bond, Table 2). In these structures, a ring closed across the pyrrolic NH and the propionic carbonyl can be defined to illustrate the feasibility of ring closure by a hydrogen bond. In the case of isomer **5**, this macrocycle has ten atoms, four of which should be almost coplanar, namely $C_8{}^1$, C_8, C_9 and C_{10}. By contrast, the more distal position of the propionic acid substituent in isomer **6** would require an 11 atom ring with five coplanar members in trans configuration. This additional ring strain may impair the formation of the pyrrolic hydrogen bond. This reason can explain the relative difference in the heats of formation (i.e. $\mathbf{5_I}$ is 3.3 kcal/mol more stable than $\mathbf{6_I}$). Suggestively, this value falls within the range of energy usually attributed to a single hydrogen bond in this class of compounds [25]. Nevertheless, the strain that prevents the existence of the innermost pyrrolic hydrogen bond would not preclude the formation of the peripheral hydroxyl/lactamic carbonyl hydrogen bond.

The resemblance between compound $\mathbf{5_I}$ and bilirubin IXα (Table 3) indicates that the position of the propionic acid substituent at C_8 in the tetrapyrrole system constitutes a critical stabilizing factor for the overall 'ridge tile' conformation of the molecule.

For each isomer, an attempt to predict the relative proportions of hydrogen-bonded versus nonhydrogen bonded conformations based on their relative molecular mechanics energy according to a Boltzmann distribution will fail, because this neglects the entropy difference. In our case, where ring closure is an issue, this term can be quite substantial. A calculation based on molecular mechanics energies alone would tend to overestimate the proportion of hydrogen bonded populations. By contrast, molecular dynamics could provide a better description of the conformational ensemble.

We adopted an MC/SD method [20], which successfully predicted the hydrogen bonding pattern of a series of Gellman's diamides [26]. This method, as applied to compounds **5** and **6** (Table 5), showed that compound **5** is indeed able to form all three intramolecular hydrogen bonds, whereas an impairment in the formation of the $CO_7{}^3...H_{23}N$ bond and a lesser impediment in the $CO_7{}^3...H_{24}N$ bond exist for compound **6**. The hydroxyl/lactamic carbonyl hydrogen bond is present in all cases. Perhaps due to its peripheral location in both molecules, this bond appears to be permissive, i.e. by itself, it does not determine any particular conformation.

In agreement with this prediction, the ^{1}H NMR evidence indicates that compound **5** does form all three hydrogen bonds, whereas in **6**, at least the pyrrolic NH

does not appear to be involved in hydrogen bonding. This feature would confer isomer **6** a more polar character than **5**.

Our theoretical calculations substantiate earlier predictions [12] on the possibility that one hydrogen bond may not be formed in the case of monopropionic bilirubins substituted at C_7. More generally, results presented here indicate that folded structures indeed exist, even when an incomplete hydrogen bonding network occurs.

A conformational search based on Monte Carlo, complemented by a combined stochastic/molecular dynamics method, provides a powerful tool to predict the molecular behavior of bilirubins.

3. Experimental

Electronic absorption spectra were determined using a Hitachi U-2000 spectrophotometer. ^{1}H NMR spectra were recorded in deuterated chloroform on a Bruker MSL 300 spectrometer. FABMS spectra of bilirubins were taken with a ZAB SEQ (VG, Fisons) spectrometer. Infrared spectra were performed with a FT-IR Bruker IFS 25 spectrometer. Melting points were determined on a Kofler melting point apparatus and were not corrected. Microanalyses were performed using a Carlo Erba EA 1108 elemental analyzer.

Bovine albumin (98–99%, w/w) was purchased from Sigma Chemical Co. All other chemicals used were of reagent grade. Solvents were distilled before use.

3.1 Synthesis of biliverdins

3.1.1 3,13,17-Triethyl-1,19,21,24-tetrahydro-2,7,12,18-tetramethyl-1,19-dioxobilin -8-propanoic acid (3); 3,13,17-triethyl-1,19,21,24-tetrahydro-2,8,12,18-tetramethyl-1,19-dioxobilin -7-propanoic acid (4)

A common procedure was used for the synthesis of the above mentioned compounds (Scheme 1). Biliverdin (**1** or **2**) (10 mg) was dissolved in tetrahydrofuran (10 ml) followed by the addition of methanol (10 ml) and of a 2 M sodium hydroxide solution (4 ml). The solution was kept in the dark under nitrogen at 37°C during 4 h for biliverdin **1**, and during 3 h for biliverdin **2**. The reaction mixture was then cooled, neutralized with glacial acetic acid and the products were extracted with dichloromethane (20 ml). The extracts were washed with water (2×10 ml), dried (Na_2SO_4), filtered, and evaporated to dryness in vacuo. Biliverdins **3** and **4** were obtained in quantitative yields and used as such for the following synthetic step, after checking their purity by TLC on silica gel plates (20×20 cm, silica gel F_{254}, 0.25 mm thick, Riedel de Haën) developed with chloroform:acetone (90:10, v/v) or chloroform:methanol:water (48:28:6, v/v).

3.2 Synthesis of bilirubins

3.2.1 3,13,17-Triethyl-1,10,19,21,23,24-hexahydro-2,7,12,18-tetramethyl-1,19-dioxo bilin-8-propanoic acid (5); 3,13,17-triethyl-1,10,19,21,23,24-hexahydro-2,8,12,18-tetramethyl-1,19-dioxobilin-7-propanoic acid (6)

A common procedure was used for the synthesis of the above mentioned compounds (Scheme 1). Sodium borohydride (10 mg) was added to a solution of biliverdin in tetrahydrofuran (10 ml) and methanol (5 ml) and the mixture was stirred in the dark at room temperature under a stream of nitrogen. After 2 h, an additional 10 mg of sodium borohydride was added and the reaction was continued for 1 h. After cooling, the solution was acidified to pH 4–5 with 1 M hydrochloric acid and extracted with dichloromethane (20 ml). The extracts were then washed with water (2×10 ml), dried (Na_2SO_4), filtered and evaporated to dryness in vacuo. The residue was then dissolved in 0.1 M sodium hydroxide and a 0.1 M hydrochloric acid solution was later added to precipitate the bilirubin. This suspension was centrifuged and the precipitate was washed twice with cold water. This procedure for crystallization was repeated once more. The overall yield of bilirubins **5** and **6** was 85–90%, starting from the methyl (or ethyl) esters **1** and **2**, respectively.

Compound **5**: R_f 0.86 (silica, $CHCl_3$:CH_3OH:H_2O, 48:28:6, v/v); mp 280°C (dec., from NaOH–HCl 0.1 M); IR (film) 3389, 2917, 1733, 1667 cm^{-1}; ^{1}H NMR ($CDCl_3$) δ 0.9 (m, 9H), 1.7 (s, 6H), 1.92 (s, 3H), 1.94 (s, 3H), 2.13 (m, 6H), 2.3 (m, 2H), 2.6 (m, 2H), 3.8 (s, 2H), 5.75 (s, 1H), 5.85 (s, 1H), 7.74 (s, NH, pyrrole), 8.7 (s, NH, pyrrole), 8.0 (s, NH, lactam), 10.35 (s, NH, lactam), 13.6 (s, 1H, CO_2H); UV-vis (nm) 410 (ε 41,744) in $CHCl_3$, 423.5 (ε 42,507) in CH_3OH; FABMS *m/z* (3-nitro-benzyl alcohol) 544 (M^+, 100%). Anal. calcd for $C_{32}H_{40}N_4O_4$ requires C, 70.56; H, 7.40; N, 10.29. Found C, 70.15; H, 7.10; N, 9.92.

Compound **6**: R_f 0.77 (silica, $CHCl_3$:CH_3OH:H_2O, 48:28:6, v/v); amorphous solid; IR (film) 3350, 2970, 1712, 1689 cm^{-1}; ^{1}H NMR ($CDCl_3$) δ 0.9 (m, 9H), 2.27 (s, 6H), 2.3 (s, 3H), 2.4 (s, 3H), 2.45 (m, 6H), 2.56 (m, 2H), 2.85 (m, 2H), 3.65 (s, 2H), 6.0 (s, 1H), 6.1 (s, 1H), 8.00 (s, NH, pyrrole), 9.98 (s, NH, pyrrole), 9.57 (s, NH, lactam), 10.25 (s, NH, lactam), 13.2 (s, 1H, CO_2H); UV-vis (nm) 392.5 (ε 45,027) in $CHCl_3$, 392 (ε 44,863) in CH_3OH; FABMS *m/z* (3-nitro-benzyl alcohol) 544 (M^+, 100%). Anal. calcd for $C_{32}H_{40}N_4O_4$ requires C, 70.56; H, 7.40; N, 10.29. Found: C, 70.80; H, 7.27; N, 10.50.

3.3 Biological experiments

3.3.1 Animals

Male Wistar rats weighing 300–350 g were obtained from the Animal House of Facultad de Farmacia y Bioquímica, Universidad de Buenos Aires.

3.3.2 Solution of pigments for infusion

Compounds **5** or **6** (0.04 mg, 73.5 nmol) were dissolved in 0.05 ml of 0.1 M sodium hydroxide and 1 ml of albumin solution (10%, w/v, of bovine albumin dissolved in 0.15 M NaCl solution) was added [6].

3.3.3 Studies on biliary excretion

The rats were kept under anesthesia with diethyl ether and the common bile duct was cannulated with 12 cm of PE-10 tubing and protected from light with an aluminum foil. The left femoral vein was also cannulated (PE-10 tubing, 12 cm) and bilirubin solution was injected into the animal via the catheter for about 1 min with a 1 ml syringe [27].

Throughout the experimental period, room temperature was 20°C and the body temperature of rats was maintained with infrared lamps. The bile was collected in tubes placed on ice, protected from light and the volume was measured during the common duct cannulation ($t = 0$ min) and at 30, 60 and 90 min after the bilirubin had been injected into the femoral vein. No significant variation in the bile flow was observed. The volume of bile fluid measured at each time point was 0.35 ± 0.05 ml. Approximately 10% of the injected bilirubins were excreted in the bile fluid.

3.4 Extraction from bile and separation of free and conjugated bilirubins

Biliary excretion of each pigment was studied on four Wistar rats. Bile samples were acidified by the addition of 8 vol. of glycine-HCl buffer (pH 1.8) followed by the addition of 2 vol. of ascorbic acid solution (100 mg/ml) saturated with sodium chloride [28]. An excess of sodium chloride was added to keep the solution saturated. The solution was then extracted several times at 0–4°C with chloroform:ethanol (1:1, v/v) [7,27,29]. The concentrated extract of each infused rat was then applied to silica gel plates (20×20 cm, silica gel F_{254}, 0.25 mm thick, Riedel de Haën), developed with chloroform:methanol:water (48:28:6, v/v). The plates were dried and the yellow bands of bilirubins and their conjugates were scraped off and eluted from the silica with methanol:water (1:1, v/v). The amount of bilirubins present in the eluates was estimated by measuring the absorbance in the range 385–430 nm for the conjugate of bilirubin **5** and for bilirubin **6**. Free bilirubin IXα and its conjugates were estimated by measuring the absorbance in the range 444–453 nm (ε 60,000) [2].

3.5 Identification of bilirubins

Solutions of free and conjugated bilirubins were evaporated under vacuum at room temperature. Bilirubin **5** monoglucuronide and bilirubin **6** were compared with reference compounds **5** and **6** by TLC on silica gel plates using chloroform:methanol:water (48:28:6, v/v) as developing solvent. After rechromatography on TLC plates, as described above, the compounds were eluted with methanol:water (1:1, v/v) and these samples were submitted to FABMS.

The structures of bilirubin IXα, its monoglucuronide and diglucuronide were confirmed by their transformation into their corresponding azopigments. Methanolysis of these azopigments was followed by analysis of their methyl esters and conjugated sugar by established procedures [4,7,28,29].

3.6 Conformational search

Molecular mechanics calculations were carried out with MacroModel 4.5 and BatchMin 4.5 [14] running on a Silicon Graphics Indigo XS24Z (R4000, 128 MB RAM, 1 GB hard disk) under the Irix 5.2 operating system. The semiempirical method AM1 was implemented in HyperChem 3.0 [15] running on a PC (Intel 486, 20 MB RAM, 1 GB hard disk) under Windows '95.

3.7 Optimized Monte Carlo search, energy minimization and relative stability of isomers

In this paper we used MM2* and AMBER* force fields (the versions of MM2 and AMBER, respectively, implemented in MacroModel [18]). By default, atomic partial charges are calculated from data in the molecular mechanics force field chosen. Both force fields use distance dependent dielectric electrostatics. The electrostatic equation used by MM2* uses partial charges and Coulomb's law, instead of the standard dipole–dipole electrostatics. MM2* includes approximate parameters for hydrogen bonds which were adjusted to mimic AMBER hydrogen bonding potentials. AMBER* is identical to authentic AMBER [30], with additions. A number of generalized parameters have been added to the field to allow qualitative modeling on many types of molecules. The field is supplied with the united-atom AMBER charge set, and Kollman's 6,12-Lennard Jones hydrogen bonding treatment [31]. The conformational search of bilirubins was carried out with an optimized Monte Carlo method [32] which employed the MM2* and AMBER* force fields, as implemented in MacroModel 4.5. Energy minimization used a conjugated gradient method, with a final gradient of 0.01 kcal/Å mol as the criterion for convergence. After the Monte Carlo steps, initial conformers were partially minimized (250 iterations), and the subset of resulting structures was further minimized until convergence. In this process, duplicate and high-energy structures were discarded. In the end, all nonenatiomeric conformers within a 6 kcal/mol window above the global minimum were tabulated. Atoms belonging to the tetrapyrrole backbone and the

propionic acid substituent were taken into account for comparisons.

In order to validate the application of this method on bilirubins, we ran a test calculation on bilirubin IXα. One hundred thousand Monte Carlo steps were carried out, starting from three different structures, namely, those which had the following values for the central pair of dihedral angles (Φ_1,Φ_2): 0,0; 180,180 and 180,0°. Ten independent degrees of freedom were considered for the Monte Carlo search, namely, the above-mentioned central pair of dihedral angles and all torsions along the propionic acid substituents.

We employed a similar protocol for the conformational search of compounds **5** and **6**, starting from structures showing (Φ_1,Φ_2): 0,0; 180,180; 0,180 and 180,0°. Eight degrees of freedom, namely, Φ_1 through Φ_8 (see Fig. 1) were considered here. Each run included 50,000 Monte Carlo steps. However, in most cases, 10,000 steps sufficed to sample the conformational ensemble.

The output conformers from the previous analysis were later optimized by the semiempirical method AM1. The protocol included a conjugated gradient method to approach the minimum and a final gradient threshold of 0.1 kcal/Å mol. A single point energy calculation on the optimized structures provided the values for the heats of formation.

The simulated annealing protocol used a time step of 1.5 fs. The temperature for the first 10 ps was set at 300 K, the next 20 ps were run at 150 K, and, finally, 20 ps were run at 50 K. In the end, the resulting structure was minimized until convergence (at 0 K) [18].

3.8 Mixed Monte Carlo/stochastic dynamics

In order to simulate the conformational ensemble of bilirubins we adopted a mixed Monte Carlo/stochastic dynamics (MC/SD) method [20]. In the course of the simulation, every SD time step is followed by an MC step. The total time in all cases was 3 ns after an initial equilibration time of 50 ps. A time step of 1.5 fs was used for the SD part. In all cases, the MC acceptance ratio was never lower than 0.3% or higher than 5%.

Two hundred thousand conformers were sampled for each compound, resulting from an MC/SD simulation run at 300 K in chloroform, employing the semi-analytical solvation treatment GB/SA [33] and the AMBER* force field parameters. The default cut-off distance of 12 Å was increased to 50 Å in the electrostatics term. Six degrees of freedom, namely, Φ_1 through Φ_6 (see Fig. 1) were considered here. No constraint was put to torsions, and not more than two dihedral angles were allowed to change at each Monte Carlo step.

A hydrogen bond is formed whenever (i) the distance between acceptor and donor is smaller than 2.5 Å, (ii) the angles N-H...O(=C) and (CO)O–H...O(=C) are greater than 120°, and (iii) the angles (N–)H...O=C and CO(O–)H...O=C are greater than 90°.

Acknowledgements

This work was supported by grants from the National Research Council (CONICET), the University of Buenos Aires and Fundación Antorchas. M. E. M. is a recipient of a graduate student fellowship from CONICET. We thank the expert technical assistance with animal handling of Mr Alejandro V. Ceccarelli and Ms Cecilia Ricciardelli. We kindly acknowledge the excellent advice of Dr D. Quentin McDonald (Columbia University).

References

[1] O'Carra P. In Smith KM, editor. Heme-cleavage: Biological systems and chemical analogs. Porphyrins and Metalloporphyrins; Amsterdam:Elsevier, 1975:123–153.
[2] Crawford JM, Ransil BJ, Potter CS, Westmoreland SV, Gollan JL. J Clin Invest 1987;79:1172.
[3] Burchell B. In Tavoloni N, Berk PD, editors. Molecular biology of the uridine diphosphate glucoronosyltranferases. Hepatic Transport and Bile Secretion Physiology and Pathophysiology. New York: Raven, 1993:489–499.
[4] Blumenthal SG, Taggart DB, Ikeda RM, Ruebner BH, Bergstrom DE. Biochem J 1977;167:535.
[5] Fevery J, Blanckaert N, Leroy R, Michiels R, Heirwegh KPM. Hepatology 1983;3:177.
[6] Blanckaert N, Heirwegh KPM, Zaman Z. Biochem J 1977;164:229.
[7] Awruch J, Mora ME, Lemberg A, Coll CT, Frydman RB. Biol Chem Hoppe-Seyler 1994;375:617.
[8] Person RV, Peterson BR, Lightner DA. J Am Chem Soc 1994;116:42, and references cited therein.
[9] McDonagh AF, Lightner DA. Cell Mol Biol 1994;40:965, and references cited therein.
[10] McDonagh AF, Lightner DA. In Bock KW, Gerock W, Matern S, editors. Hepatic Metabolism and Disposition of Endo and Xenobiotics, Proceedings of the Falk Symposium No. 57. Dordrecht (The Netherlands): Kluwer, 1991:47–59.
[11] Awruch J. Frydman B. Tetrahedron 1986;42:4137.
[12] Holmes DL, Lightner DA. J. Heterocyclic Chem 1995;32:113.
[13] Trull FR, Franklin RW, Lightner DA. J. Heterocyclic Chem 1987;24:1573, and references cited therein.
[14] Mohamadi F, Richards NGJ, Guida WC, Liskamp R, Lipton M, Caufield C, Chang G, Hendrickson T, Still WC. J. Comput Chem 1990;11:440.
[15] HyperChem for Windows, developed by and licensed from Hypercube Inc., Autodesk, Inc., 1992.
[16] Bonnett R, Davies JE, Hursthouse NB, Sheldrick GM. Proc R Soc London, Ser. B. 1978;202:249.
[17] LeBas G, Allegret A, Mauguen Y, DeRango C, Bailly M. Acta Crystallogr, Sect. B 1980;B36:3007.
[18] MacroModel, A Primer, Version 4.5, Department of Chemistry, Columbia University, New York, NY 10027, 1994.

[19] Shelver WL, Rosemberg H, Shelver WH. Intl. J. Quantum Chem 1992;44:141.
[20] Guarnieri F, Still WC. J Comp Chem 1994;15:1302.
[21] Tiribelli C, Ostrow D. Hepatology 1993;17:715.
[22] Falk H, Grubmayr K, Holbacher G, Hofer O, Leodolter A, Neufingerl F, Ribo JM. Monatsh Chem 1977;108:1113.
[23] Kaplan D, Navon G. Isr J Chem 1983;23:177.
[24] Hwang K, Timothy Anstine D, Lightner DA. Tetrahedron 1994;50:9919.
[25] Boiadjiev SE, Person RV, Puzicha G, Knobler C, Maverick E, Trueblood KN, Lightner DA. J Am Chem Soc 1992;114:10123.
[26] McDonald DQ, Still WC. J Am Chem Soc 1994;116:11550.
[27] Mora ME, Bari SE, Awruch J. Bioorg Med Chem Lett 1997;7:1249.
[28] Blanckaert N, Fevery J, Heirwegh KPM, Compernolle F. Biochem J 1977;164:237.
[29] Awruch J, Lemberg A, Frydman RB, Frydman B. Biochim Biophys Acta 1982;714:209.
[30] Weiner SJ, Kollman PA, Case DA, Singh UC, Ghio C, Alagona G, Profeta Jr. S, Weiner P. J Am Chem Soc 1984;106:765.
[31] Ferguson DM, Kollman PA. J Comput Chem 1990;12:620.
[32] Chang G, Guida WC, Still WC. J Am Chem Soc 1989;111:4379.
[33] Still WC, Tempczyk A, Hawley RC, Hendrickson T. J Am Chem Soc, 1990;112:6127.